7

Multi-Camera Visual Servoing of a Micro Helicopter Under Occlusions

Yuta Yoshihata, Kei Watanabe, Yasushi Iwatani and Koichi Hashimoto
Tohoku University
Japan

1. Introduction

Autonomous control of unmanned helicopters has the advantage that there is no need to develop skilled workers and has potential for surveillance tasks in dangerous areas including forest-fire reconnaissance and monitoring of volcanic activity. For vehicle navigation, the use of computer vision as a sensor is effective in unmapped areas. Visual feedback control is also suitable for autonomous takeoffs and landings, since precise position control is required at a neighborhood of the launch pad or the landing pad. Such applications have generated considerable interest in the vision based control community (Altug et al., 2005; Amidi et al., 1999; Ettinger et al., 2002; Mahony & Hamel, 2005; Mejias et al., 2006; Proctor et al., 2006; Saripalli et al., 2003; Shakernia et al., 2002; Wu et al., 2005; Yu et al., 2006).

The authors have developed a visual control system for a micro helicopter (Watanabe et al., 2008). The helicopter does not have any sensors that measure its position or posture. Two cameras are placed on the ground. They track four black balls attached to rods connected to the bottom of the helicopter. The differences between the current ball positions and given reference positions in the camera frames are fed to a set of PID controllers. It is not required that sensors for autonomous control are installed on the helicopter body, and we need no mechanical or electrical improvements of existing unmanned helicopters that are controlled remotely and manually.

In visual control, tracked objects have to be visible in the camera views, but tracking may fail due to occlusions. An occlusion occurs when an object moves across in front of a camera or when the background color happens to be similar to the color of a tracked object. Multicamera systems are suitable for designing a robust controller under occlusions, since even when a tracked object is not visible in a camera view, the other cameras may track it. The visual control system with two cameras proposed in (Yoshihata et al., 2007) is robust against temporary occlusions. If an occlusion is detected in a camera view then the other camera is used to control the helicopter. The positions of the invisible tracked objects in the image plane of the occluded camera are estimated by using the positions in the other image plane. The control method proposed in (Yoshihata et al., 2007) is called the camera selection approach in this paper.

This paper proposes another switched visual feedback control method that is called the image feature selection approach. It is robust against temporary and partial occlusions even

Source: Visual Servoing, Book edited by: Rong-Fong Fung,
ISBN 978-953-307-095-7, pp. 234, April 2010, INTECH, Croatia, downloaded from SCIYO.COM

when a tracked object is not visible in any of the camera views. We also use two cameras and two tracked objects for each camera. This configuration is redundant for helicopter control, but it is suitable for making a control system robust against occlusions. This paper assumes that at most one tracked object is occluded at each time, as a first step towards a unified framework that combines the image feature selection approach presented in this paper and the camera selection approach proposed in (Yoshihata et al., 2007). The errors between the current positions of the tracked objects and pre-specified references are used to compute the control input signals, when all the tracked objects are visible. If one of the tracked objects is invisible, then the controller uses the errors given by the other three tracked objects. The position of the occluded object is also estimated by using the other three tracked objects.

2. Experimental setup

The experimental system considered in this paper consists of a small helicopter and two stationary cameras as illustrated in Fig. 1. The helicopter does not have any sensors that measure the position or posture. It has four small black balls, and they are attached to rods connected to the bottom of the helicopter. The black balls are indexed from 1 to 4. The two cameras are placed on the ground and they look upward. Snapshots of the helicopter from the two cameras can be seen in Fig. 2. The camera configuration and the use of the redundant tracked objects enable a robust controller design under temporary and partial occlusions as described in Section 6.

The system takes 8.5 milli-seconds to make the control input signals from capturing images of the balls. This follows from the use of fast IEEE 1394 cameras, Dragonfly Express[1].

The small helicopter used in experiments is X. R. B–V2–lama developed by HIROBO (see Fig. 3). It has a coaxial rotor configuration. The two rotors share the same axis, and they rotate in opposite directions. The tail is a dummy. A stabilizer is installed on the upper rotor head. It mechanically keeps the posture horizontal.

Table 1 summarizes specifications of the system.

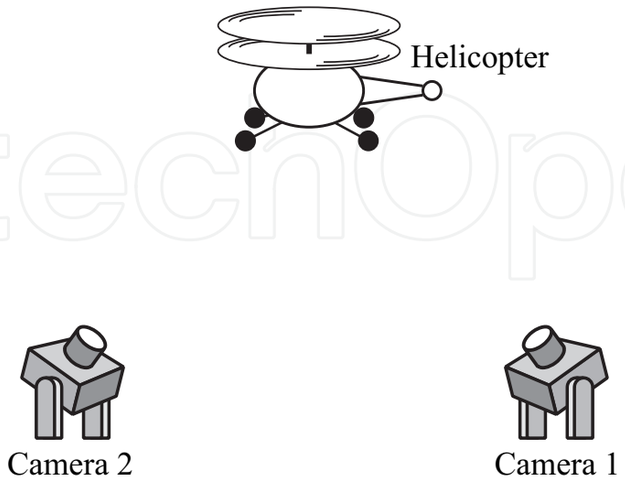

Fig. 1. System configuration.

[1] Dragonfly Express is a trademark of Point Grey Research Inc.

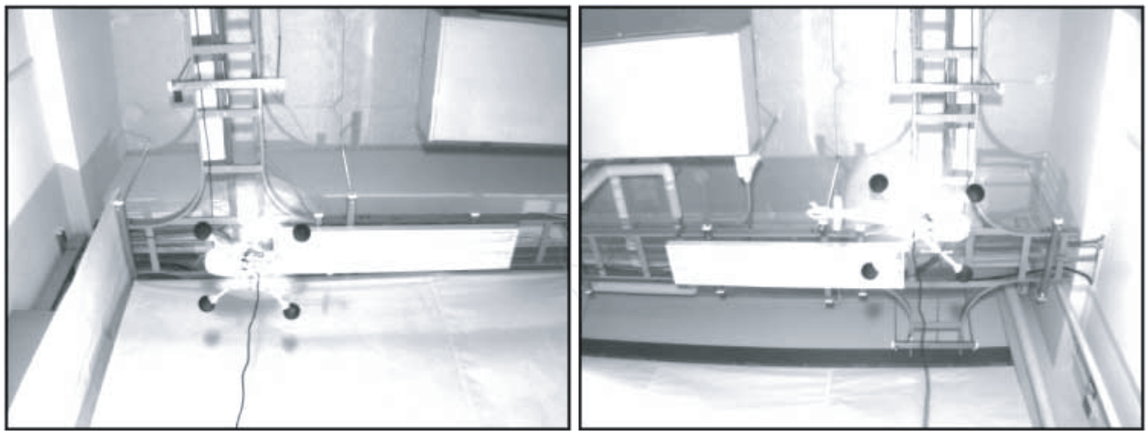

Fig. 2. Snapshots of the helicopter. The right one was captured from camera 1 and the left one from camera 2. The helicopter was controlled manually.

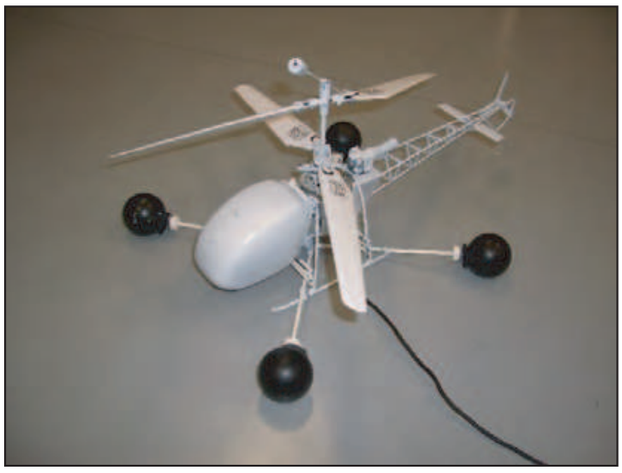

Fig. 3. X.R.B. with four black balls.

Length of the helicopter,	0.40 [m].
Height of the helicopter,	0.20 [m].
Rotor length of the helicopter,	0.35 [m].
Weight of the helicopter,	0.22 [kg].
Focal length of the lens,	0.0045 [m].
Camera resolution,	640 × 480 [pixels].
Pixel size,	7.4 [μm] × 7.4 [μm].

Table 1. Specifications of the system.

3. Mathematical preliminaries

3.1 Coordinate frames

Let Σ^w be the world reference frame and a coordinate frame Σ^b be attached to the helicopter body as illustrated in Fig. 4. The z^w axis is directed vertically downward. A coordinate frame

Σ^j is attached to camera j for j = 1, 2. The z^j axis lies along the optical axis of camera j. The axes x^w, x^1 and x^2 are parallel. The coordinate frame $x^j y^j$ corresponds to the image frame of camera j, and it is denoted by Σ^{cj}.

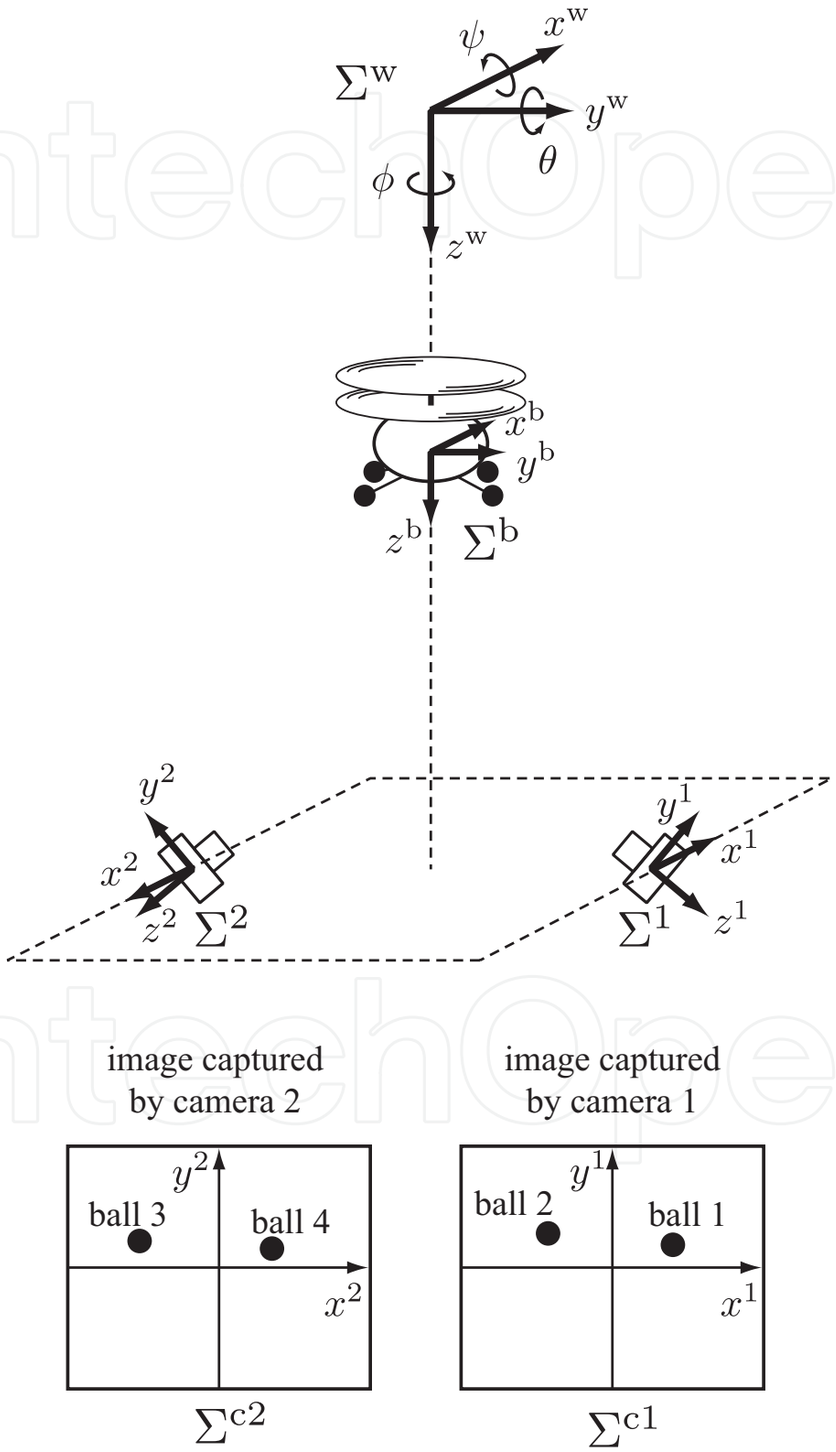

Fig. 4. Coordinate frames.

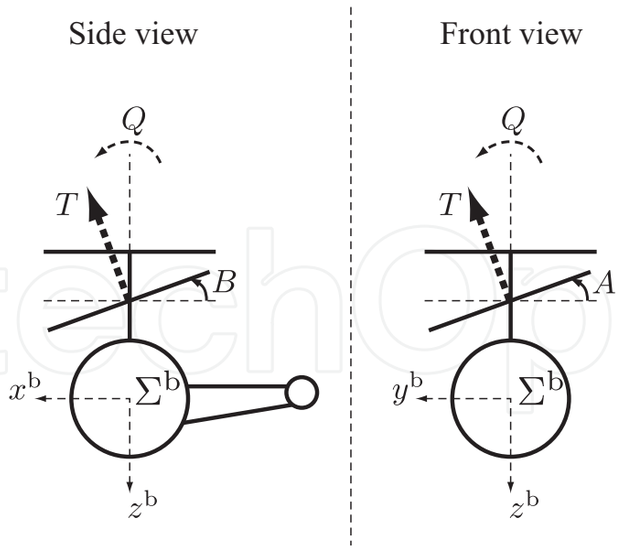

Fig. 5. The helicopter coordinate frame and input variables.

The helicopter position relative to the world reference frame Σ^{w} is denoted by (x, y, z). The roll, pitch and yaw angles are denoted by ψ, θ, φ, respectively. The following four variables are individually controlled by signals supplied to the transmitter (see Fig. 5):

B : Elevator, pitch angle of the lower rotor.

A : Aileron, roll angle of the lower rotor.

T : Throttle, resultant force of the two rotor thrusts.

Q : Rudder, difference of the two torques generated by the two rotors.

The corresponding input signals are denoted by V_B, V_A, V_T and V_Q. Note that x, y, z and ϕ are controlled by applying V_B, V_A, V_T and V_Q, respectively.

3.2 Mathematical preliminaries

In this paper, we make the following four assumptions:

1. It is supposed that

$$\theta(t) = 0, \psi(t) = 0, \forall\, t \geq 0, \tag{1}$$

   where recall that θ denotes the angle about y^{w} axis and ψ the angle about x^{w} axis.
2. The reference position relative to the world reference frame Σ^{w} is always set to $\mathbf{0}$. When the reference position is changed, the world reference frame is replaced and the reference position is set to the origin of the new world reference frame.
3. Camera 1 captures images of balls 1 and 2, and camera 2 takes images of balls 3 and 4.
4. At most one tracked object is occluded at each time.

Recall that the helicopter has the horizontal-keeping stabilizer. Both the angles θ and ψ converge to zero fast enough even when the body is inclined. Thus, the first assumption is not far from the truth in practice. We here define

$$\boldsymbol{r} = \begin{bmatrix} x & y & z & \phi \end{bmatrix}^{\mathrm{T}}. \tag{2}$$

Note that $\boldsymbol{r}$ means the vector of the generalized coordinates. Then, our goal is that $\boldsymbol{r}(t) \rightarrow \mathbf{0}$ as $t \rightarrow \infty$ from the first and second assumptions.

The third and fourth assumptions are made to consider a simple example in which visible image features should be selected from redundant features under temporary and partial occlusions. The assumptions are suitable for a first step towards a unified framework that combines the image feature selection approach presented in this paper and the camera selection approach proposed in (Yoshihata et al., 2007).

4. Image Jacobian

This section derives the image Jacobian that gives a relationship between the vector of the generalized coordinates $\boldsymbol{r}$ and the vector of the image features.
The position of the center of gravity of ball i in the image frame is denoted by $\boldsymbol{\xi}_i = [\xi_{ix}, \xi_{iy}]^\mathsf{T} \in \mathbb{R}^2$ for $i = 1, \ldots, 4$. We define

$$\boldsymbol{\zeta}_0 = \begin{bmatrix} \boldsymbol{\xi}_1^\mathsf{T} & \boldsymbol{\xi}_2^\mathsf{T} & \boldsymbol{\xi}_3^\mathsf{T} & \boldsymbol{\xi}_4^\mathsf{T} \end{bmatrix}^\mathsf{T}. \tag{3}$$

In addition, we set

$$\boldsymbol{\zeta}_i = \begin{bmatrix} \boldsymbol{\xi}_{\sigma_{i1}}^\mathsf{T} & \boldsymbol{\xi}_{\sigma_{i2}}^\mathsf{T} & \boldsymbol{\xi}_{\sigma_{i3}}^\mathsf{T} \end{bmatrix}^\mathsf{T}, \tag{4}$$

for $i = 1, \ldots, 4$, where

$$\sigma_{ik} \in \{1,2,3,4\} / \{i\}, \quad k = 1,2,3, \tag{5}$$

$$\sigma_{i1} < \sigma_{i2} < \sigma_{i3}. \tag{6}$$

The vector $\boldsymbol{\zeta}_0$ is used as the vector of image features, when all positions of the tracked balls can be measured correctly. On the other hand, $\boldsymbol{\zeta}_i$ for $i = 1, 2, 3, 4$ implies the vector of visible image features when ball i is occluded. They enable us to give a switched controller that is robust against occlusions, if the fourth assumption holds or equivalently at most one tracked object is occluded. Details will be discussed in the next section.
Let ${}^\mathrm{b}\boldsymbol{p}_i \in \mathbb{R}^3$ denote the position of ball i in the frame Σ^b. The position of ball i in the frame Σ^j is denoted by

$$\boldsymbol{p}_i = \begin{bmatrix} x_i & y_i & z_i \end{bmatrix}^\mathsf{T} \in \mathbb{R}^3, \tag{7}$$

where $j = 1$ for $i = 1, 2$ and $j = 2$ for $i = 3, 4$. We have

$$\begin{bmatrix} \boldsymbol{p}_i \\ 1 \end{bmatrix} = {}^j\boldsymbol{H}_\mathrm{w}(\boldsymbol{r})\,{}^\mathrm{w}\boldsymbol{H}_\mathrm{b}(\boldsymbol{r}) \begin{bmatrix} {}^\mathrm{b}\boldsymbol{p}_i \\ 1 \end{bmatrix}, \tag{8}$$

where ${}^j\boldsymbol{H}_\mathrm{w}(\boldsymbol{r})$ and ${}^\mathrm{w}\boldsymbol{H}_\mathrm{b}(\boldsymbol{r})$ are the homogeneous transformation matrices from Σ^w to Σ^j and from Σ^b to Σ^w, respectively (see for example (Spong et al., 2005) for deriving the homogeneous transformation matrices). It then holds that

$$|z_i| \begin{bmatrix} \boldsymbol{\xi}_i \\ 1 \end{bmatrix} = \boldsymbol{F} \begin{bmatrix} \boldsymbol{p}_i \\ 1 \end{bmatrix} \tag{9}$$

where

$$\boldsymbol{F} = \begin{bmatrix} f & 0 & 0 & 0 \\ 0 & f & 0 & 0 \\ 0 & 0 & 1 & 0 \end{bmatrix}, \tag{10}$$

and f is the focal length of the lens (see for example (Ma et al., 2004) for the camera model). It is straightforward to verify that

$$\boldsymbol{\xi}_i = \frac{f}{|z_i|} \begin{bmatrix} x_i \\ y_i \end{bmatrix}$$

$$=: \boldsymbol{\alpha}_i(\boldsymbol{r}). \tag{11}$$

We here define

$$\boldsymbol{\beta}_0(\boldsymbol{r}) = \begin{bmatrix} \boldsymbol{\alpha}_1^{\mathrm{T}}(\boldsymbol{r}) & \boldsymbol{\alpha}_2^{\mathrm{T}}(\boldsymbol{r}) & \boldsymbol{\alpha}_3^{\mathrm{T}}(\boldsymbol{r}) & \boldsymbol{\alpha}_4^{\mathrm{T}}(\boldsymbol{r}) \end{bmatrix}^{\mathrm{T}}, \tag{12}$$

$$\boldsymbol{\beta}_i(\boldsymbol{r}) = \begin{bmatrix} \boldsymbol{\alpha}_{\sigma_{i1}}^{\mathrm{T}}(\boldsymbol{r}) & \boldsymbol{\alpha}_{\sigma_{i2}}^{\mathrm{T}}(\boldsymbol{r}) & \boldsymbol{\alpha}_{\sigma_{i3}}^{\mathrm{T}}(\boldsymbol{r}) \end{bmatrix}^{\mathrm{T}}, \tag{13}$$

for $i = 1, \ldots, 4$, where σ_{i1}, σ_{i2} and σ_{i3} are defined by (5) and (6). The equations (12) and (13) provide transformations from the generalized coordinates $\boldsymbol{r}$ to the image features ζ_i.
We define

$$\boldsymbol{J}_i = \left. \frac{\partial \boldsymbol{\beta}_i}{\partial \boldsymbol{r}} \right|_{\boldsymbol{r}=\boldsymbol{0}}. \tag{14}$$

Then it holds that

$$\dot{\boldsymbol{\zeta}}_i = \boldsymbol{J}_i \dot{\boldsymbol{r}}, \tag{15}$$

at $\boldsymbol{r} = 0$. Each $\boldsymbol{J}_i$ ($i = 0, \ldots, 4$) is referred to as the image Jacobian.

5. Controller design

This paper proposes a switched visual feedback control system illustrated in Fig. 6, where $\boldsymbol{\xi}_i^{\mathrm{ref}}$ denotes the image reference of ball i relative to the corresponding image frame Σ^{cj} and

$$\boldsymbol{\zeta}_0^{\mathrm{ref}} = \begin{bmatrix} \boldsymbol{\xi}_1^{\mathrm{ref}\,\mathrm{T}} & \boldsymbol{\xi}_2^{\mathrm{ref}\,\mathrm{T}} & \boldsymbol{\xi}_3^{\mathrm{ref}\,\mathrm{T}} & \boldsymbol{\xi}_4^{\mathrm{ref}\,\mathrm{T}} \end{bmatrix}^{\mathrm{T}}, \tag{16}$$

$$\boldsymbol{\zeta}_i^{\mathrm{ref}} = \begin{bmatrix} \boldsymbol{\xi}_{\sigma_{i1}}^{\mathrm{ref}\,\mathrm{T}} & \boldsymbol{\xi}_{\sigma_{i2}}^{\mathrm{ref}\,\mathrm{T}} & \boldsymbol{\xi}_{\sigma_{i3}}^{\mathrm{ref}\,\mathrm{T}} \end{bmatrix}^{\mathrm{T}}, \tag{17}$$

for $i = 1, \ldots, 4$, where σ_{i1}, σ_{i2} and σ_{i3} are defined by (5) and (6). The system is an image-based visual servo system, since the proposed controller uses the image Jacobian derived in the previous section and the errors between the vector of the image features $\zeta_i(t)$ and the corresponding given reference ζ_i^{ref} to obtain the input signals. Image-based visual servo control is robust against model uncertainties (Hashimoto, 2003).

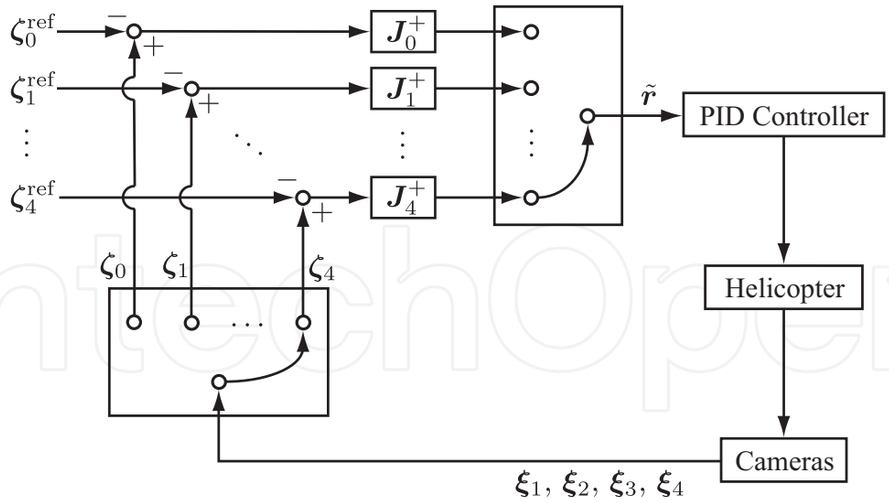

Fig. 6. Closed loop system.

The switch in the closed loop depends on which image feature $\boldsymbol{\xi}_i$ is invisible. The decision of switching will be described in Section 5.2. In this paper, the image feature $\boldsymbol{\xi}_i$ is labeled as 'normal', when the system decides that $\boldsymbol{\xi}_i$ is measured correctly. Similarly, $\boldsymbol{\xi}_i$ is labeled as 'occluded', when the system decides that $\boldsymbol{\xi}_i$ is not measured correctly.

5.1 Measurement of image features

An image feature $\boldsymbol{\xi}_i(t)$ (i = 1, . . . ,4) is given by the following manner. A binary data matrix at time t is first obtained from an image captured by camera j, and it is denoted by $\boldsymbol{I}_j(x^j,y^j)$ for j = 1, 2. The matrix $\boldsymbol{I}_j(x^j,y^j)$ has values of 1 for black and 0 for white. We then make a search window $\mathbb{S}_i$ whose center is defined as follows:

Normal case: It is set at $\boldsymbol{\xi}_i(t-h)$, where h denotes the sampling time.
Occluded case: We estimate $\boldsymbol{\xi}_i(t)$ by

$$\boldsymbol{J}_0\boldsymbol{J}_i^+(\boldsymbol{\zeta}_i(t)-\boldsymbol{\zeta}_i^{\mathrm{ref}})+\boldsymbol{\zeta}_0^{\mathrm{ref}} =: \begin{bmatrix}\tilde{\boldsymbol{\xi}}_1^{\mathsf{T}} & \tilde{\boldsymbol{\xi}}_2^{\mathsf{T}} & \tilde{\boldsymbol{\xi}}_3^{\mathsf{T}} & \tilde{\boldsymbol{\xi}}_4^{\mathsf{T}}\end{bmatrix}^{\mathsf{T}}, \tag{18}$$

where $\boldsymbol{J}_i^+$ denotes the Moore-Penrose inverse of $\boldsymbol{J}_i^+$. The center is set at $\tilde{\boldsymbol{\xi}}_i$.
The size of the window $\mathbb{S}_i$ is given by a constant. We define an image data matrix by

$$\bar{\boldsymbol{I}}_{ji}(x^j,y^j)=\begin{cases}\boldsymbol{I}_j(x^j,y^j), & for\ (x^j,y^j)\in\mathbb{S}_i,\\ 0, & otherwise,\end{cases}$$

where j = 1 for i = 1, 2 and j = 2 for i = 3, 4. The image feature $\boldsymbol{\xi}_i(t)$ is the center of mass of $\bar{\boldsymbol{I}}_{ji}(x^j,y^j)$.

5.2 Selection of image features

Let three constants δ, $m_{\min}$ and $m_{\max}$ be given. Let $m_i(t)$ denote the area, or equivalently the zero-th order moment, of the image data $\bar{\boldsymbol{I}}_{ji}(x^j,y^j)$. An occlusion is detected or cancelled for each image feature $\boldsymbol{\xi}_i(t)$ in the following manner.

Normal case: If $m_{\min} \le m_i(t) \le m_{\max}$ holds, then $\boldsymbol{\xi}_i(t)$ is labeled as 'normal' again. Otherwise, it is labeled as 'occluded'.
Occluded case: If it holds that $m_{\min} \le m_i(t) \le m_{\max}$ and

$$\| \boldsymbol{J}_0^+(\boldsymbol{\zeta}_0(t) - \boldsymbol{\zeta}_0^{\text{ref}}) - \boldsymbol{J}_i^+(\boldsymbol{\zeta}_i(t) - \boldsymbol{\zeta}_i^{\text{ref}}) \| < \delta, \tag{19}$$

then $\boldsymbol{\xi}_i(t)$ is labeled as 'normal'. Otherwise, it is labeled as 'occluded' again.
If $\boldsymbol{\xi}_i(t)$ is occluded for i, then $\boldsymbol{\zeta}_i(t)$ is used at the next step. Otherwise, or equivalently if every image feature $\boldsymbol{\xi}_i(t)$ is normal, then $\boldsymbol{\zeta}_0$ is used at the next step.

5.3 Control input voltages

We compute

$$\tilde{\boldsymbol{r}}(t) = \begin{bmatrix} \tilde{x}(t) & \tilde{y}(t) & \tilde{z}(t) & \tilde{\phi}(t) \end{bmatrix}^{\mathsf{T}}$$

$$:= \boldsymbol{J}_i^+(\boldsymbol{\zeta}_i(t) - \boldsymbol{\zeta}_i^{\text{ref}}), \tag{20}$$

for $\boldsymbol{\zeta}_i$ selected in the previous subsection. The input signals are given by a set of PID controllers of the form

$$V_B(t) = b_1 - P_1\tilde{x} - I_1\int_0^t \tilde{x}\,\mathrm{d}t - D_1\dot{\tilde{x}}, \tag{21}$$

$$V_A(t) = b_2 - P_2\tilde{y} - I_2\int_0^t \tilde{y}\,\mathrm{d}t - D_2\dot{\tilde{y}}, \tag{22}$$

$$V_T(t) = b_3 - P_3\tilde{z} - I_3\int_0^t \tilde{z}\,\mathrm{d}t - D_3\dot{\tilde{z}}, \tag{23}$$

$$V_Q(t) = b_4 - P_4\tilde{\phi} - I_4\int_0^t \tilde{\phi}\,\mathrm{d}t - D_4\dot{\tilde{\phi}}, \tag{24}$$

where b_i, P_i, I_i and D_i are constants for $i = 1, \ldots, 4$.

6. Experiment and result

The world reference frame Σ^w and the camera frames Σ^1 and Σ^2 are located as shown in Fig. 7. The controller gains are tuned to the values in Table 2. The positions of the four black balls in the frame Σ^b are given by

$${}^b\boldsymbol{p}_1 = \begin{bmatrix} 0.1 & 0.1 & 0.04 \end{bmatrix}^{\mathsf{T}}, \tag{25}$$

$${}^b\boldsymbol{p}_2 = \begin{bmatrix} -0.1 & 0.1 & 0.04 \end{bmatrix}^{\mathsf{T}}, \tag{26}$$

$${}^b\boldsymbol{p}_3 = \begin{bmatrix} 0.1 & -0.1 & 0.04 \end{bmatrix}^{\mathsf{T}}, \tag{27}$$

$${}^b\boldsymbol{p}_4 = \begin{bmatrix} -0.1 & -0.1 & 0.04 \end{bmatrix}^{\mathsf{T}}. \tag{28}$$

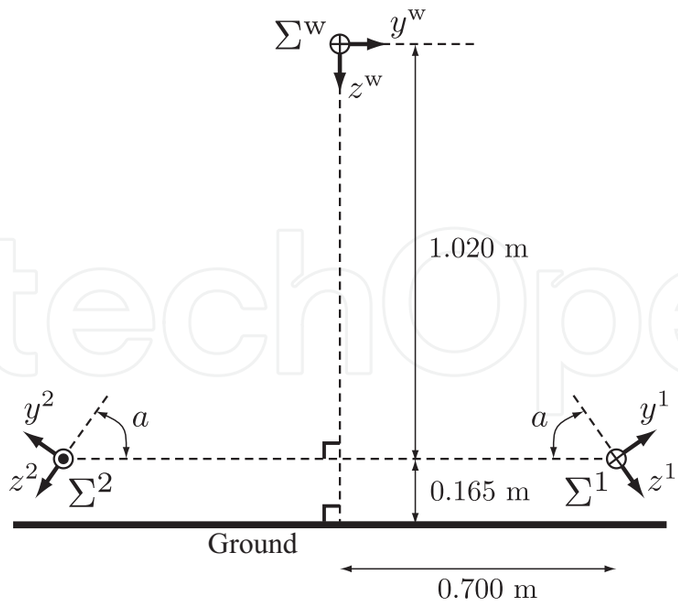

Fig. 7. Locations of the world reference frame Σ^{w} and the camera frames Σ^1 and Σ^2. The angle a is set to $a = 11\pi/36$.

	b_i	P_i	I_i	D_i
V_B	3.47	3.30	0.05	2.60
V_A	3.38	3.30	0.05	2.60
V_T	2.70	1.90	0.05	0.80
V_Q	1.92	3.00	0.05	0.08

Table 2. PID gains.

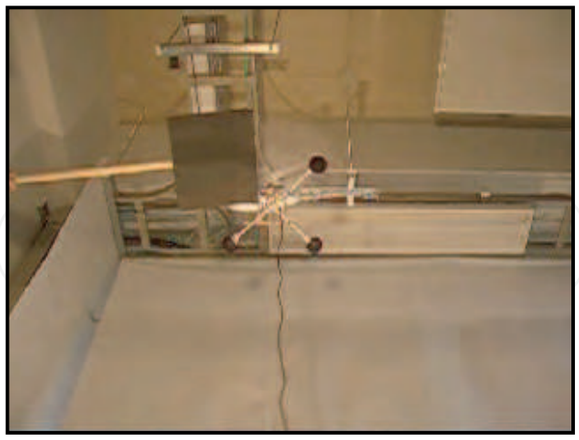

Fig. 8. A snapshot of helicopter flight under an occlusion. This was captured by a camera placed next to camera 2. Ball 3 was not captured correctly at this moment.

The image reference ζ_0^{ref} is set to

$$\zeta_0^{ref} = \begin{bmatrix} 84.6 & 10.5 & -21.1 & 16.1 & -65.6 & 41.9 & 43.4 & 40.9 \end{bmatrix}^{\mathrm{T}}, \text{ (pixels).} \tag{29}$$

This was obtained by an actual measurement.
Ball 1 or 3 was occluded temporarily and intentionally. Long time occlusions for around 10 seconds were presented twice for each ball. Short time occlusions were done four times for each ball, and they were successively done from ball 3 to 1. A snapshot of helicopter flight under an occlusion can be seen at Fig. 8.
Fig. 9 shows the x positions of balls 1 and 3 in the corresponding image planes. When an occlusion is detected, the value is set at –150 in the figure to make the plot easy to read. For example, ξ_3 was labeled 'occluded' from 15 to 25 seconds. It is seen that the number of occlusion detection is equivalent to the number of intentional occlusions.

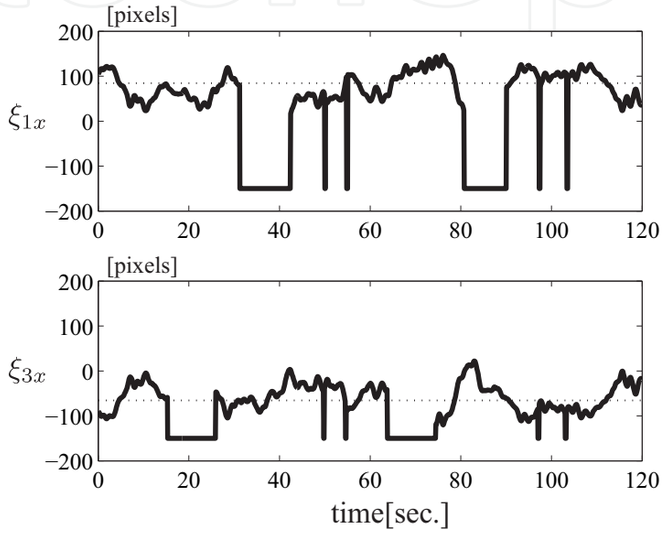

Fig. 9. Experimental result. Solid lines: Time profiles of the positions of image features. When an occlusion is detected, the value is set to –150. Dotted lines: Given references.

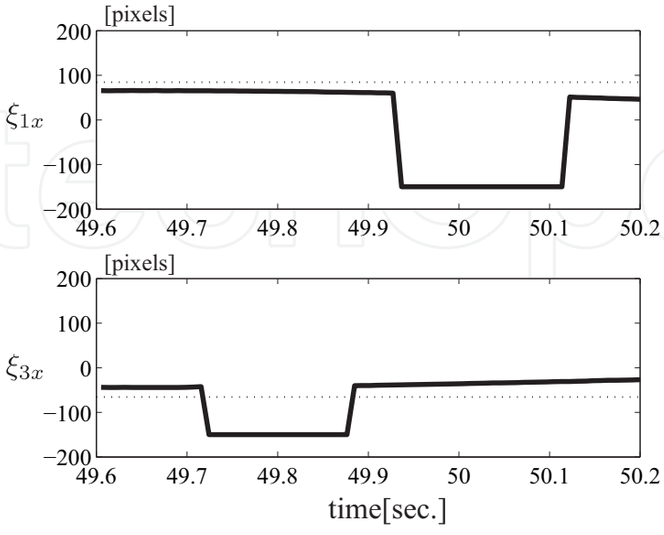

Fig. 10. Experimental result: Time profiles of the positions of image features. This is a closeup of Fig. 9 between 49.6 and 50.2 seconds.

Fig. 10 illustrates a closeup of Fig. 9 between 49.60 and 50.20 seconds. An occlusion is detected for ball 3 from 49.72 to 49.88 seconds. After 50 milli-seconds, an occlusion is detected for ball 1. Our system deals with such rapid change, since high-speed cameras are used.

Fig. 11 shows the generalized coordinates $\tilde{\boldsymbol{r}}$ defined by (20). It is seen that the helicopter hovered in a neighborhood of the reference position. In particular, the z position is within 7 [cm] for all time.

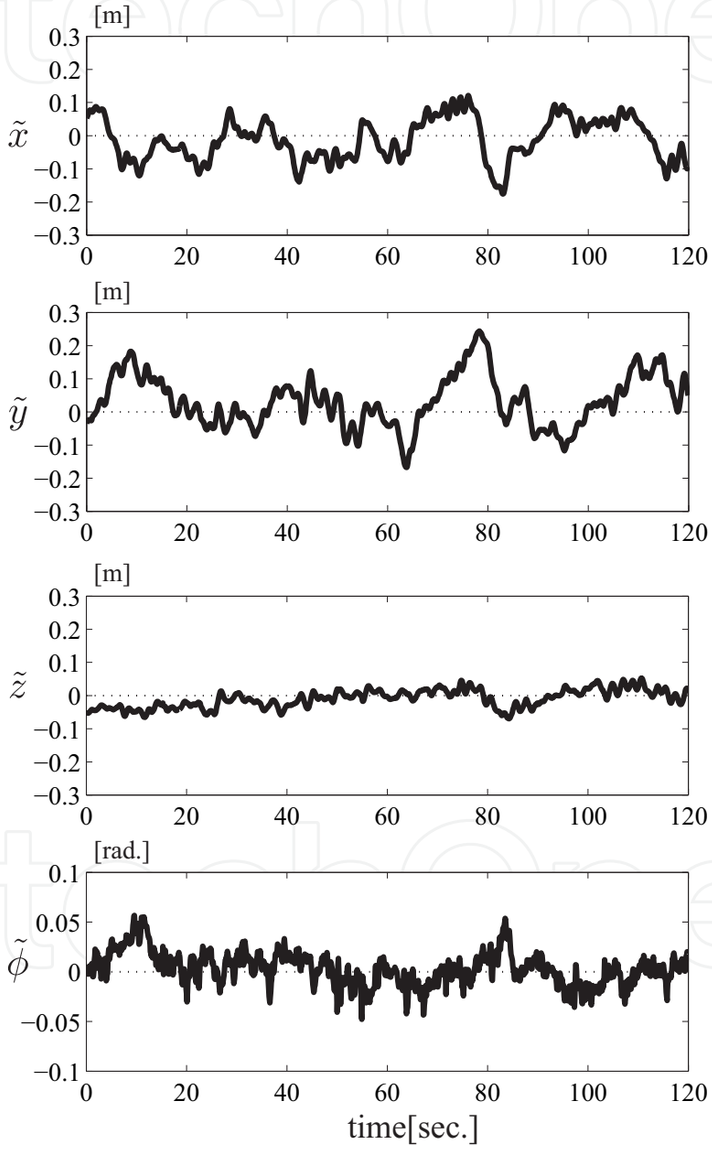

Fig. 11. Experimental result: Time profile of the generalized coordinates $\tilde{\boldsymbol{r}}$.

Several movies can be seen at http://www.ic.is.tohoku.ac.jp/E/research/ helicopter/. They show stability, convergence and robustness of the system in an easy-to-understand way, while the properties may not be seen easily from the figures shown here.

7. Conclusion

This paper has presented a visual control system that enables a small helicopter to hover under temporary and partial occlusions. Two stationary and upward-looking cameras track four black balls attached to rods connected to the bottom of the helicopter. The differences between the current tracked object positions and pre-specified reference positions are fed to a set of PID controllers, when all the tracked objects are visible. If an occlusion is detected for a tracked object, the controller uses the errors given by the other three tracked objects. The system can keep the helicopter in a stable hover, and the proposed method is robust to temporary and partial occlusions even when a tracked object is not visible in any of the camera views.

8. References

Altug, E., Ostrowski, J. P. & Taylor, C. J. (2005). Control of a quadrotor helicopter using dual camera visual feedback, *International Journal of Robotics Research* 24(5): 329–341.

Amidi, O., Kanade, T. & Fujita, K. (1999). A visual odometer for autonomous helicopter flight, *Robotics and Autonomous Systems* 28: 185–193.

Ettinger, S. M., Nechyba, M. C., Ifju, P. G. & Waszak, M. (2002). Vision-guided flight stability and control for micro air vehicles, *Proc. IEEE/RSJ International Conference on Intelligent Robots and Systems*, Lausanne, Switzerland, pp. 2134–2140.

Hashimoto, K. (2003). A review on vision-based control of robot manipulators, *Advanced Robotics* 17(10): 969–991.

Ma, Y., Soatto, S., Koˇseck´a, J. & Sastry, S. S. (2004). *An Invitation to 3-D Vision: From Images to Geometric Models*, Springer-Verlag.

Mahony, R. & Hamel, T. (2005). Image-based visual servo control of aerial robotic systems using linear image features, *IEEE Trans. on Robotics* 21(2): 227–239.

Mejias, L. O., Saripalli, S., Cervera, P. & Sukhatme, G. S. (2006). Visual servoing of an autonomous helicopter in urban areas using feature tracking, *Journal of Field Robotics* 23(3): 185–199.

Proctor, A. A., Johnson, E. N. & Apker, T. B. (2006). Vision-only control and guidance for aircraft, *Journal of Field Robotics* 23(10): 863–890.

Saripalli, S., Montgomery, J. F. & Sukhatme, G. S. (2003). Visually-guided landing of an unmanned aerial vehicle, *IEEE Trans. on Robotics and Automation* 19(3): 371–381.

Shakernia, O., Sharp, C. S., Vidal, R., Shim, D. H., Ma, Y. & Sastry, S. (2002). Multiple view motion estimation and control for landing an unmanned aerial vehicle, *IEEE International Conference on Robotics and Automation*, Washington, DC, pp. 2793–2798.

Spong, M. W., Hutchinson, S. & Vidyasagar, M. (2005). *Robot Modeling and Control*,Wiley.

Watanabe, K., Yoshihata, Y., Iwatani, Y. & Hashimoto, K. (2008). Image-based visual PID control of a micro helicopter using a stationary camera, *Advanced Robotics* 22(2-3): 381– 393.

Wu, A. D., Johnson, E. N. & Proctor, A. A. (2005). Vision-aided inertial navigation for flight control, *AIAA Guidance, Navigation and Control Conference and Exhibit*, San Francisco, California, pp. 1669–1681.

Yoshihata, Y., Watanabe, K., Iwatani, Y. & Hashimoto, K. (2007). Visual control of a micro helicopter under dynamic occlusions, *The 13th International Conference on Advanced Robotics*, Jeju, Korea, pp. 785–790. Also, in Lee, S., Suh, I. H., & Kim, M. S., editors,

Recent Progress in Robotics: Viable Robotic Service to Human, pp. 185–197. LNCIS, Springer-Verlag (2008).

Yu, Z., Celestino, D. & Nonami, K. (2006). Development of 3D vision enabled small-scale autonomous helicopter, *2006 IEEE/RSJ International Conference on Intelligent Robots and Systems*, Beijing, Chaina, pp. 2912–2917.

Visual Servoing

Edited by Rong-Fong Fung

ISBN 978-953-307-095-7

Hard cover, 234 pages

Publisher InTech

Published online 01, April, 2010

Published in print edition April, 2010

The goal of this book is to introduce the visional application by excellent researchers in the world currently and offer the knowledge that can also be applied to another field widely. This book collects the main studies about machine vision currently in the world, and has a powerful persuasion in the applications employed in the machine vision. The contents, which demonstrate that the machine vision theory, are realized in different field. For the beginner, it is easy to understand the development in the vision servoing. For engineer, professor and researcher, they can study and learn the chapters, and then employ another application method.

How to reference

In order to correctly reference this scholarly work, feel free to copy and paste the following:

Yuta Yoshihata, Kei Watanabe, Yasushi Iwatani and Koichi Hashimoto (2010). Multi-Camera Visual Servoing of a Micro Helicopter Under Occlusions, Visual Servoing, Rong-Fong Fung (Ed.), ISBN: 978-953-307-095-7, InTech, Available from: http://www.intechopen.com/books/visual-servoing/multi-camera-visual-servoing-of-a-micro-helicopter-under-occlusions

INTECH
open science | open minds

InTech Europe
University Campus STeP Ri
Slavka Krautzeka 83/A
51000 Rijeka, Croatia
Phone: +385 (51) 770 447
Fax: +385 (51) 686 166
www.intechopen.com

InTech China
Unit 405, Office Block, Hotel Equatorial Shanghai
No.65, Yan An Road (West), Shanghai, 200040, China
中国上海市延安西路65号上海国际贵都大饭店办公楼405单元
Phone: +86-21-62489820
Fax: +86-21-62489821

IntechOpen